SCIENCE CHINA
Chemistry

•ARTICLES•

February 2024 Vol.67 No.2: 732–740
https://doi.org/10.1007/s11426-023-1840-y

SAPO-34 facilitates the formation of benzene, toluene and xylenes in direct syngas conversion over $MnCrO_x$-SAPO-34-ZSM-5

Shuchi Zhang[1,2], Dengyun Miao[1,2*], Yi Ding[1,2], Mengyuan Li[1,2], Shujing Guo[3], Yujuan Zhang[3], Xiulian Pan[1,2*] & Xinhe Bao[1,2]

[1]*State Key Laboratory of Catalysis, Dalian Institute of Chemical Physics, Chinese Academy of Sciences, Dalian 116023, China;*
[2]*University of Chinese Academy of Sciences, Beijing 100049, China;*
[3]*Shaanxi Yanchang Petroleum (Group) Co., Ltd., & Dalian Institute of Chemical Physics Xi'an Clean Energy (Chemical Industry) Research Institute, Xi'an 710000, China*

Received July 7, 2023; accepted October 14, 2023; published online November 2, 2023

Direct conversion of syngas to aromatics over metal oxide and zeolite (OXZEO) composite catalysts is promising. However, the selectivity of more valuable products such as benzene, toluene and xylenes (BTX) is limited due to undesired secondary methylation of BTX. Herein, we report that the introduction of SAPO-34 into $MnCrO_x$-ZSM-5 catalyst enhances significantly the formation of BTX without sacrificing the aromatics selectivity. Under optimized conditions, the fraction of BTX in aromatics reaches 64.7% *versus* 28.9% over the catalyst without SAPO-34. A number of model reaction tests and characterizations reveal that SAPO-34 consumes partially the intermediates such as ketene, by converting them to light olefins. Thus, the methylation of BTX by ketene to heavy aromatics is inhibited over the external acid sites of ZSM-5, leading to an enhanced BTX selectivity in the products. This hybrid catalyst provides an efficient method for highly selective synthesis of BTX from syngas.

selective syngas conversion, OXZEO, aromatics, BTX, multi-functional catalysts

Citation: Zhang S, Miao D, Ding Y, Li M, Guo S, Zhang Y, Pan X, Bao X. SAPO-34 facilitates the formation of benzene, toluene and xylenes in direct syngas conversion over $MnCrO_x$-SAPO-34-ZSM-5. *Sci China Chem*, 2024, 67: 732–740, https://doi.org/10.1007/s11426-023-1840-y

1 Introduction

Aromatics, especially benzene, toluene and xylenes, so called BTX, are very important basic chemicals, which are the raw materials for synthetic plastics, fuels, pesticides and other functional materials. Currently, BTX is mainly produced from crude oil. It is highly desirable to develop a procedure for the BTX production from non-petroleum resources, such as coal, natural gas and biomass. Syngas (CO/H_2) is an important platform for the utilization of these non-petroleum carbon resources and it can be converted to aromatics *via* the intermediate stage of methanol synthesis [1–4]. Although the technology of Fischer–Tropsch synthesis (FTS) can convert syngas directly, it mainly leads to products of straight-chain hydrocarbons [5–9]. Alternatively, metal oxide–zeolite (OXZEO)-based bifunctional catalysts were demonstrated to be active for direct syngas conversion to aromatics. Different combinations of metal oxide and ZSM-5 zeolite have been reported, including $ZnCrO_x$ [10], $FeZnCrO_x$ [11], $ZnZrO_x$ [12], Cr_2O_3 [13,14], $CeZrO_x$ [15], $MoZrO_x$ [16], MnO [17], $ZnMnO_x$ [18], $MnCrO_x$ [19]. A selectivity over 70% was frequently reported. However, the aromatic products are dominated by heavy aromatics, such as C_9 and C_{10} aromatics, and the selectivity of more valuable BTX is generally lower than 35%. There were efforts to increase BTX selectivity by shielding the external acid sites of ZSM-5 zeolite, since C_9 and C_{10} aromatic compounds were considered to be formed by methylation of BTX generated in the

*Corresponding authors (email: dengyunmiao@dicp.ac.cn; panxl@dicp.ac.cn)

micropores of ZSM-5. For instance, the BTX fraction in aromatics increased from 30% to 63% over tetraethylorthosilane (TEOS)-modified ZSM-5 [12]. However, this generally requires repetitive and tedious steps to modify the zeolites with a delicate layer of silica. Studies show that this silica layer has to be thick enough to shield well the external acid sites but thin enough to avoid blocking the mouth of the micropores and hence inhibiting the diffusion of the aromatic compounds [19,20]. Recently, we reported a new strategy for the selective synthesis of BTX from syngas [19]. By packing a dealkylation component, such as beta and ultra-stable zeolite Y (USY), below a catalyst bed of MnCr-ZSM-5 composite, the BTX fraction in aromatics reached over 80%. Unfortunately, the catalyst suffered deactivation because of the coke deposition on the dealkylation catalyst bed [19].

We noticed that a high selectivity of BTX was reported during the aromatization of olefins/paraffins [21]. This could be attributed to the absence of methylation reagent during the reaction. Inspired by this, we wonder if the BTX selectivity over the OXZEO catalyst can be improved by decreasing the concentration of active methylation reagent, such as ketene [22,23], methanol [12,15,16], or dimethyl ether [24], while increasing the concentration of olefins/paraffins during the reaction. Therefore, we introduce SAPO-34 into the $MnCrO_x$-ZSM-5 composite because SAPO-34 is selective in the light olefins' formation in syngas conversion and CO_2 hydrogenation [23,25–28]. The results validate that the BTX fraction in aromatics does increase significantly, from 28.9% to as high as 64.7%, and BTX selectivity among hydrocarbons reaches 41.9% *versus* 20.9% over the parent catalyst.

2 Results and discussion

2.1 Characterization of catalysts

Figure S1a shows the X-ray powder diffraction (XRD) patterns of the fresh MnCr oxide and MnCr oxide after syngas conversion. It indicates that the fresh MnCr oxide was a mixture of Mn_2O_3 and Cr_2O_3. Mn_2O_3 was reduced to MnO after syngas conversion. The adsorption–desorption isotherm of MnCr oxide in Figure S1b indicates a type IV behavior, indicating that MnCr oxide had mesopores. The specific surface area of fresh MnCr oxide was 25 $m^2\ g^{-1}$.

The XRD patterns in Figure S1c indicate that the AlPO-34 and SAPO-34 with different SiO_2/Al_2O_3 were successfully synthesized [29,30]. The ammonia temperature-programmed desorption (NH_3-TPD) profiles in Figure 1a indicate that AlPO-34 only shows an obvious peak at around 150 °C, which is attributed to NH_3 desorbing from the weak acid sites. By introducing silicon (SAPO-34), another peak centered at around 300 °C–350 °C appears, corresponding to the desorption of NH_3 from the strong acid sites. The density of the strong acid sites increases with the increasing silicon

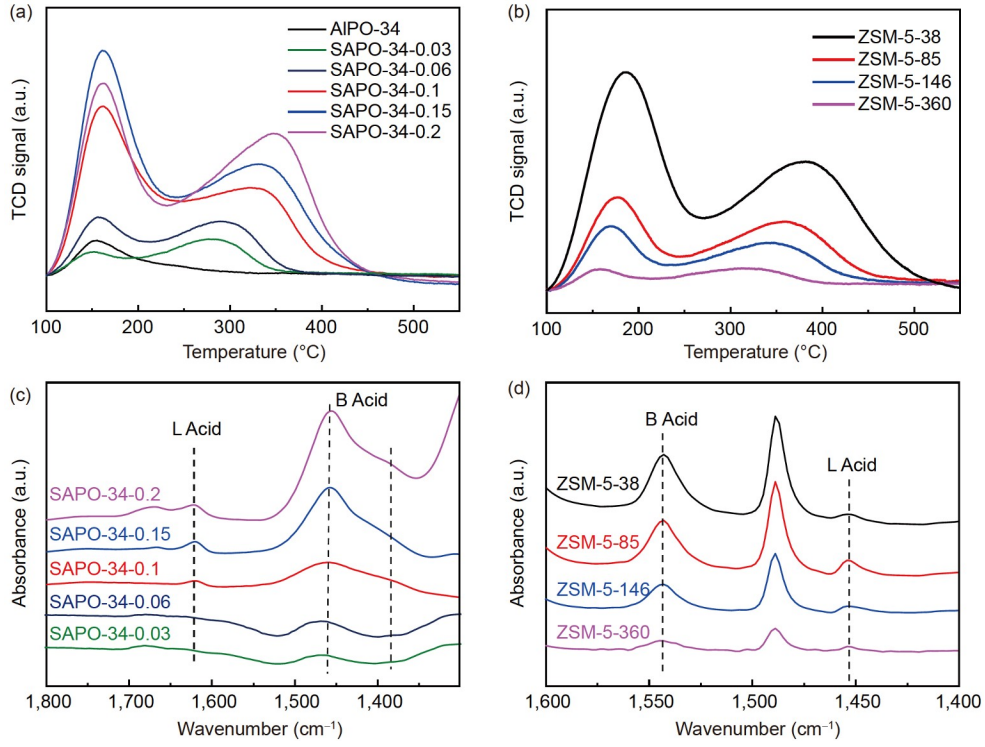

Figure 1 NH_3-TPD and IR profiles. (a) NH_3-TPD of AlPO-34 and SAPO-34, and (b) NH_3-TPD of ZSM-5. (c) NH_3-IR profiles of SAPO-34. (d) Py-IR profiles of ZSM-5 (color online).

Table 1 Acidic property of SAPO-34 and ZSM-5

Sample	Density of strong acid sites (μmol g^{-1}) [a]	B/L ratio [b]	Density of strong Brønsted acid sites (μmol g^{-1}) [c]
AlPO-34	0	/	0
SAPO-34-0.03	129.0	∞	129.0
SAPO-34-0.06	220.0	∞	229.0
SAPO-34-0.1	472.8	28.2	456.6
SAPO-34-0.15	622.6	25.2	598.8
SAPO-34-0.2	735.3	30.0	711.6
ZSM-5-38	602.4	16.0	567.0
ZSM-5-85	278.2	5.0	231.8
ZSM-5-146	189.4	5.2	158.9
ZSM-5-360	73.7	4.7	60.8

a) Corresponding to the NH_3-TPD peak centering at around 300 °C–400 °C. b) The ratio of Brønsted acid sites to Lewis acid sites, calculated according to a method reported previously [32,33]. c) Calculated according to the density of strong acid sites and the B/L ratio.

content in SAPO-34, from 129 to 735 μmol g^{-1} with the SiO_2/Al_2O_3 increasing from 0.03 to 0.2 (Table 1). All the ZSM-5 samples show the typical MFI topology (Figure S1d) [31]. Similar to SAPO-34, the NH_3-TPD profiles of ZSM-5 in Figure 1b also show two typical NH_3 desorption peaks, with the one centering around 300 °C–400 °C attributed to the strong acid sites. The density of strong acid sites of different samples is listed in Table 1, which decreases with the increasing SiO_2/Al_2O_3 in ZSM-5.

To discriminate the Brønsted acid sites (B acid) and Lewis acid sites (L acid) in SAPO-34, infrared (IR) spectra upon NH_3 adsorption (NH_3-IR) were recorded. As shown in Figure 1c, three absorption bands appeared in the region of 1,650–1,350 cm^{-1} for SAPO-34. The one around 1,620 cm^{-1} can be ascribed to the Lewis acid sites, while the other two around 1,458 cm^{-1} and 1,410 cm^{-1} are ascribed to the Brønsted acid sites [32]. The ratio of Brønsted acid sites to Lewis acid sites (B/L ratio) was calculated according to an established method [32]. The results show that all the SAPO-34 samples show a similar B/L ratio, varying between 25 and 30 (Table 1). To determine the Brønsted acid sites and Lewis acid sites over ZSM-5, pyridine instead of NH_3, was used as the probe molecule for IR analysis (Py-IR). As shown in Figure 1d, the peak centering at 1,450 cm^{-1} is ascribed to the pyridine being adsorbed on the Lewis acid sites and the one at 1,540 cm^{-1} to the Brønsted acid sites [33]. All the ZSM-5 samples exhibit a similar B/L ratio of 5, except ZSM-5-38, which shows an apparently higher B/L of 16. Based on the NH_3-TPD and NH_3-IR/Py-IR discussed above, the density of strong Brønsted acid sites was estimated. As shown in Table 1, it increases with the increasing SiO_2/Al_2O_3 ratio of SAPO-34, while decreases the with the increasing SiO_2/Al_2O_3 ratio of ZSM-5.

2.2 Enhanced BTX formation by SAPO-34

To investigate the effect of SAPO-34 on the formation of BTX in syngas conversion, a number of reference experiments were carried out. As shown in Figure S2, MnCr-SAPO-34 gives a selectivity of light olefins ($C_2^=$–$C_4^=$) in hydrocarbons 70.4% at 12.3% CO conversion. In comparison, MnCr-ZSM-5 leads to the formation of aromatics with a selectivity of 72.4 % at 13.3% CO conversion (Figure 2a). When SAPO-34 with a different amount is added into MnCr-ZSM-5 catalyst, CO conversion and CO_2 selectivity are not affected (Figure 2a). The selectivity of aromatics in hydrocarbons (Aro./HCs) is not reduced significantly either (Figure 2a). Interestingly, the fraction of BTX in aromatics (BTX/Aro.) increases and it doubles from 28.9 to 61.1% when the mass ratio of SAPO-34 to ZSM-5 is 1/1 (Figure 2b). Figure 2c highlights that the desired BTX fraction significantly increases and the undesired heavy aromatic compounds A_{9+} decreases significantly by referring to those obtained over MnCr-ZSM-5.

To evaluate the effects of SAPO-34 in-depth, we estimated the aromatization capability by calculating the selectivity of aromatic rings (carbon atom based), denoted as C_R, and the methylation capability by calculating the selectivity of the side chains of aromatics (higher than xylenes), denote as S_{Methy}, according to equations (1) and (2), respectively. The ratio of S_{Methy} to C_R (S_{Methy}/C_R) reflects the activity of BTX methylation. Figure 2d shows that the addition of SAPO-34 has little effect on aromatization, as C_R keeps almost unchanged when the ratio of SAPO-34 to ZSM-5 increases from 0/1 to 2/1. However, S_{Methy}/C_R halves from 0.15 (SAPO-34/ZSM-5 = 0/1) to 0.07 (SAPO-34/ZSM-5 = 1/1), indicating significantly inhibited methylation of BTX. Further increasing the SAPO-34/ZSM-5 ratio (2/1) does not further inhibit methylation but levels off.

$$C_R = \frac{\sum_0^x C_{6+x}H_{2x+6} \times 6}{\sum_1^n n \times c_n H_m} \times 100\% \quad (1)$$

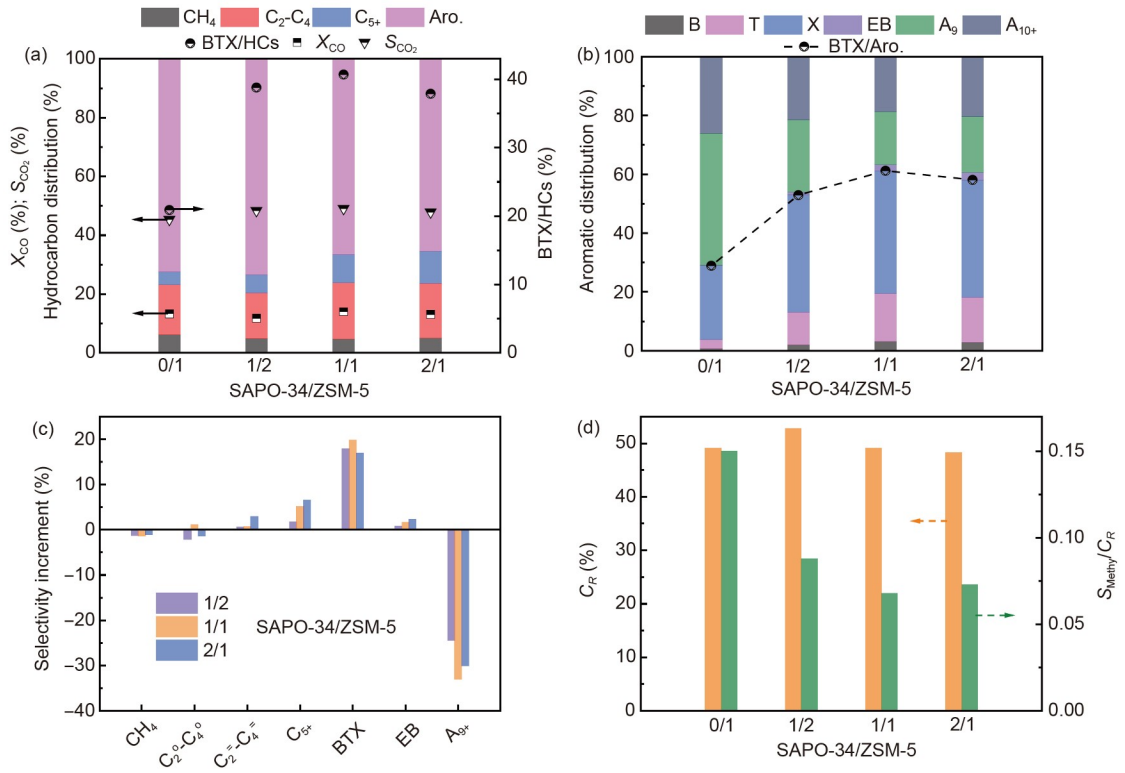

Figure 2 Effects of SAPO-34 addition on the syngas conversion. (a) Catalytic performance as a function of SAPO-34 to ZSM-5 ratio (mass ratio). (b) Distribution of aromatics. (c) Variation of product distribution compared with that obtained over the MnCr-ZSM-5 parent catalyst. (d) C_R and S_{Methy}/C_R. Reaction conditions: MnCr/zeolite = 1/3, H_2/CO/Ar = 47.5/47.5/5, 430 °C, 4.0 MPa, gas hourly space velocity (GHSV) = 2,250 mL g^{-1} h^{-1}. (C_2^o–C_4^o = light paraffins; $C_2^=$–$C_4^=$ = light olefins; B = benzene; T = toluene; X = xylenes; EB = ethylbenzene; A_9 representing aromatic compounds containing 9 carbon atoms, A_{9+} representing aromatic compounds containing 9 and more than 9 carbon atoms; A_{10+} representing aromatic compounds containing 10 and more than 10 carbon atoms; C_{5+} standing for C_{5+} aliphatic compounds.) SAPO-34 and ZSM-5 were SAPO-34-0.1 (SiO_2/Al_2O_3 = 0.1) and ZSM-5-360 (SiO_2/Al_2O_3 = 360), respectively (color online).

$$S_{\text{Methy}} = \frac{\sum_3^x C_{6+x}H_{2x+6} \times 6}{\sum_1^n n \times c_n H_m} \times 100\% \quad (2)$$

Since syngas is mainly converted to light olefins with 70.4% selectivity over MnCr-SAPO-34, we investigated the conversion of light olefins over ZSM-5, with butene as a probe molecule. Figure S3 shows a selectivity of aromatics of 40%, which is much lower than that obtained in syngas conversion over ternary MnCr-SAPO-34-ZSM-5. Further experiment of butene conversion with the CO co-feeding (Figure S3) shows that the selectivity of aromatics only increases slightly to 45%. It indicates that the remarkably increased BTX selectivity in the presence of SAPO-34 in syngas conversion is not attributed to the olefin aromatization either alone or promotion by CO over ZSM-5. There must be other factors playing roles.

2.3 The role of SAPO-34 in syngas conversion over MnCr-SAPO-34-ZSM-5 catalyst

MnCr oxide, ZSM-5 and SAPO-34 were loaded in different modes to clarify the role of SAPO-34 in syngas conversion. The results are shown in Figure 3 and Table S1. When MnCr and ZSM-5 are milled and mixed in 20–40 mesh (Mode 1), the selectivity of aromatics (Aro./HCs) is 72.4%. The addition of SAPO-34 granules either with the same size (Mode 2) or milled together with MnCr-ZSM-5 (Mode 3) gives similar overall performance with an almost the same CO conversion and slightly decreased aromatics selectivity (Aro./HCs) (72.4% *vs*. 67.9%), as displayed in Figure 3a. However, the BTX fraction (BTX/Aro.) rises from 29% to 41.2% in Mode 2 (Figure 3b) and further up to 61.1% in Mode 3. The corresponding aromatization capability (C_R) is not affected whereas S_{Methy}/C_R decreases from 0.15 to 0.07 (Figure 3c), validating that aromatization is not affected while the methylation of BTX is suppressed in the presence of SAPO-34. Thus, it leads to a significantly improved BTX fraction in aromatics. This effect is much more obvious with an intimate contact between SAPO-34 and MnCr-ZSM-5.

By contrast, ZSM-5 granules mixed either with milled MnCr-SAPO-34 (Mode 4) or arranged in dual catalyst beds (Mode 5) inhibit the aromatization significantly. For instance, the selectivity of aromatics dramatically decreases to 29% (Mode 4) and further drops to only 8% (Mode 5). These data demonstrate that the light olefins generated over MnCr-SAPO-34 cannot be converted to aromatics over the sub-

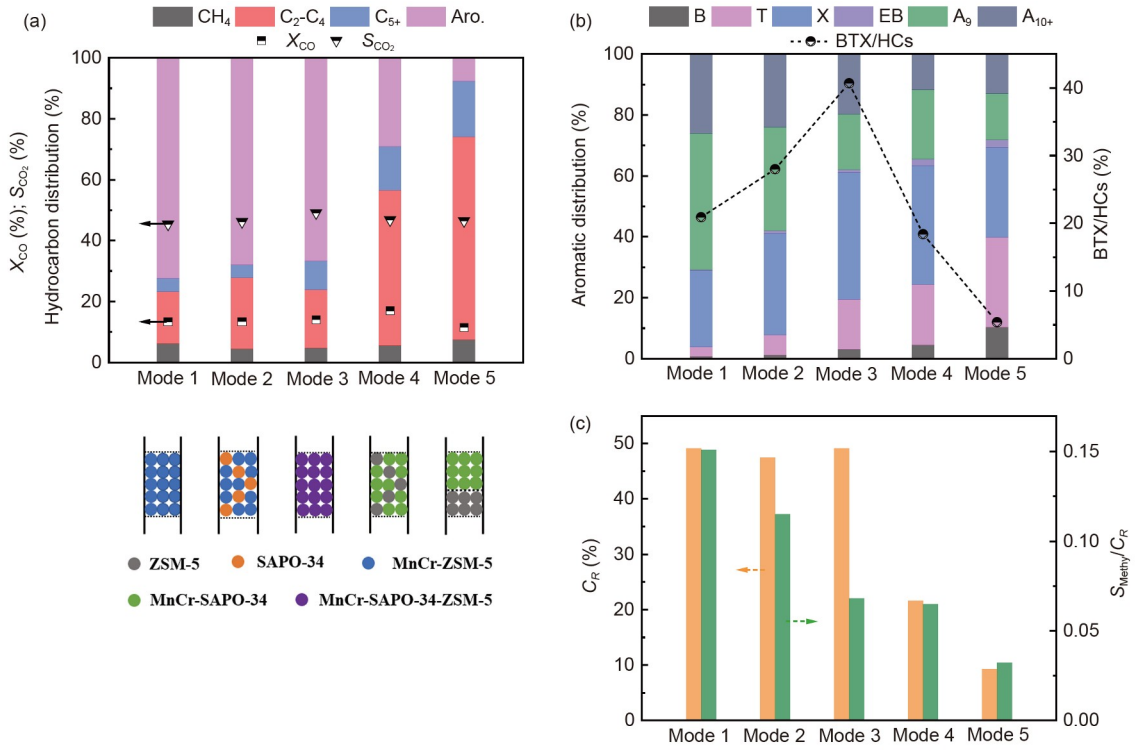

Figure 3 Catalytic performance over MnCr-SAPO-34-ZSM-5 under different catalyst packing modes. (a) Syngas conversion and product distribution. (b) Distribution of aromatic compounds. (c) C_R and S_{Methy}/C_R. Mode 1: MnCr-ZSM-5 (mill-mixed MnCr and ZSM-5). Mode 2: MnCr-ZSM-5+SAPO-34 (granule mixed MnCr-ZSM-5 and SAPO-34). Mode 3: MnCr-SAPO-34-ZSM-5 (mill-mixed MnCr, SAPO-34 and ZSM-5). Mode 4: MnCr-SAPO-34+ZSM-5 (mill-mixed MnCr and SAPO-34, being granule mixed with ZSM-5). Mode 5: MnCr-SAPO-34//ZSM-5 (mill-mixed MnCr and SAPO-34, being stacked up ZSM-5). SAPO-34 and ZSM-5 were SAPO-34-0.1 (SiO_2/Al_2O_3 = 0.1) and ZSM-5-360 (SiO_2/Al_2O_3 = 360), respectively (color online).

sequent ZSM-5 catalyst bed of the same size granules. Nor can they be converted by the homogeneously mixed ZSM-5 granules (Mode 4). Instead, most light olefins are hydrogenated to form light paraffins (Mode 4-5 in Figure 3a and Table S1) [34]. This further confirms that the remarkably increased BTX selectivity in the presence of SAPO-34 in the syngas conversion is not attributed to the aromatization of olefins.

Our previous study revealed that CO and H_2 are activated over metal oxides forming ketene as the intermediate [23]. To clarify the role of SAPO-34, we further carried out the syngas conversion with meta-xylene (MX) co-feeding as a probe reaction. As shown in Figure 4a, by co-feeding MX with syngas over MnCr-ZSM-5, the selectivity of aromatic hydrocarbons reaches 98.7% and the fraction of trimethylbenzene and heavier aromatics (A_9 and A_{10+}) is dominated (61.9%). It indicates that ketene intermediates formed on the MnCr oxide mainly react with MX as methylation agents giving dominant trimethylbenzene as products. Wang *et al.* [35] demonstrated by theoretical calculations that ketene acted as the methylation agent during C–C coupling in zeolites. By contrast, over MnCr-SAPO-34-ZSM-5, the fraction of trimethylbenzene and heavier aromatics in aromatic compounds is significantly reduced to 36.4% (Figure 4a). Since SAPO-34 readily catalyzes ketene conversion to light olefins. Thus the concentration of ketene is kept low to inhibit the methylation of xylene over the external surface of ZSM-5 zeolite (Figure 4b). It consequently leads to a significantly increased BTX selectivity over the ternary MnCr-SAPO-34-ZSM-5 composite catalyst.

2.4 Matching the multi-functionality of the different components

The cooperation of different functionalities over the tandem catalyst is the key to achieve optimum performance, such as the activity of individual steps. This is controlled by the activity of metal oxides and zeolites, and their mass ratio in OXZEO catalysts. Therefore, we varied the acid site density of SAPO-34 and ZSM-5 over the MnCr-SAPO-34-ZSM-5, and investigated their roles. As shown in Figure S4a, the density of Brønsted acid sites of SAPO-34 has little effect on the CO conversion and CO_2 selectivity over MnCr-SAPO-34-ZSM-5, but it modulates the hydrocarbon distribution (Figure 5a). Particularly, the BTX fraction among aromatics (BTX/Aro.) increases stepwise with the density of Brønsted acid sites. By contrast, the addition of AlPO-34 (MnCr-AlPO-34-ZSM-5), which has the same topology with SAPO-34 but without strong Brønsted acid sites (Table 1), gives

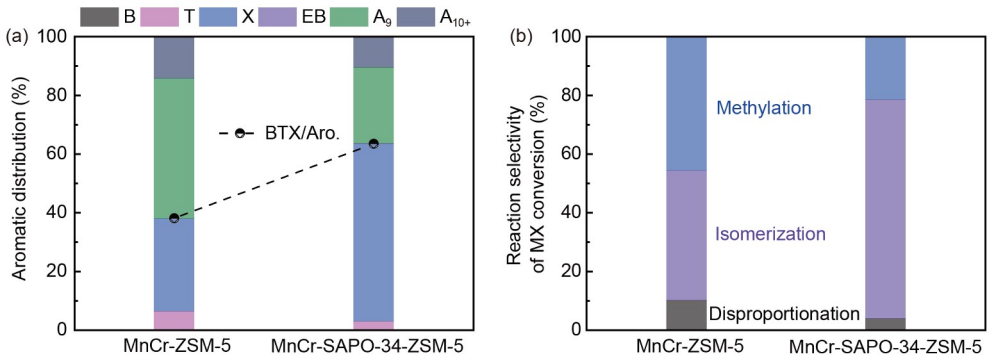

Figure 4 Syngas conversion with MX co-feeding over MnCr-ZSM-5 and MnCr-SAPO-34-ZSM-5. (a) Distribution of aromatic compounds. (b) Selectivity of methylation, isomerization and disproportionation (color online).

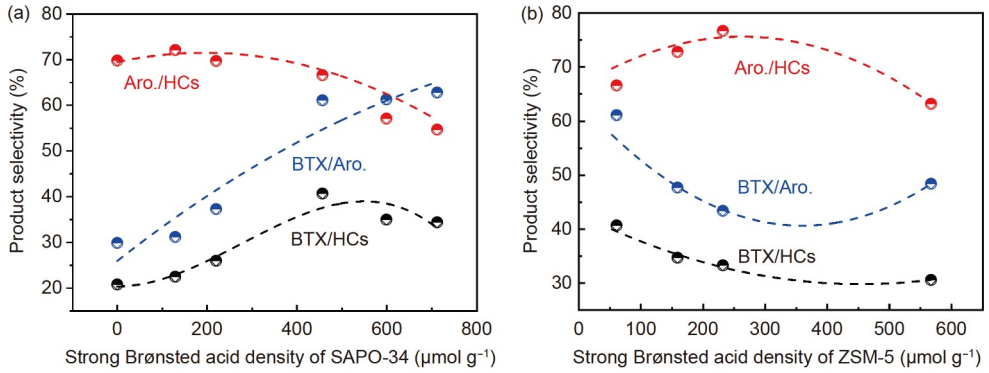

Figure 5 Effects of Brønsted acid sites density of (a) SAPO-34 and (b) ZSM-5 in syngas conversion over MnCr-SAPO-34-ZSM-5. Reaction conditions: 4.0 MPa, 430 °C, GHSV = 2,250 mL g^{-1} h^{-1}, H_2/CO/Ar = 47.5/47.5/5, MnCr/SAPO-34/ZSM-5 = 1/1.5/1.5 (color online).

69.8% aromatics selectivity (Aro./HCs) with only 29.9% BTX fraction among aromatics (BTX/Aro.). These values are similar with those obtained over MnCr-ZSM-5 (Mode 1 in Figure 3 and Table S1), showing little effect of AlPO-34. As the Brønsted acid sites have been demonstrated to be the active sites for ketene conversion [22,23,36–38], the presumption of a higher activity over zeolite with more Brønsted acid sites should be reasonable. With more ketenes being converted on SAPO-34 with more acid sites, the ketene concentration during the reaction may be kept lower and consequently the methylation of BTX by ketenes will be inhibited, leading to an enhanced BTX fraction. This explained well the correlation of BTX fraction (BTX/Aro.) with the density of Brønsted acid sites of AlPO-34 and SAPO-34 (Figure 5a). Figure 5a shows that SAPO-34-0.1 gives the highest BTX selectivity of 40.7% in hydrocarbons. However, further increasing the strong Brønsted acid site density of SAPO-34 facilitates the hydrogenation of olefins, leading to the formation of light paraffins (Table S2), which unfortunately cannot be transformed to BTX by ZSM-5 under the reaction condition. This, on the contrary, lowers the selectivity of aromatics (Aro./HCs) .

Similarly, the Brønsted acid site density of ZSM-5 has little effect on the CO conversion and CO_2 selectivity over MnCr-SAPO-34-ZSM-5 (Figure S4b) but affects the hydrocarbon distribution. As shown in Figure 5b, the aromatic selectivity (Aro./HCs) increases gradually from 66.6% to 76.7% with the density of strong Brønsted acid sites of ZSM-5 increasing from 60.8 to 231.8 μmol g^{-1}. This can be attributed to the enhanced aromatization reaction with the increasing strong Brønsted acid sites. However, it decreases to 63.2% when the density of strong Brønsted acid sites further increases to 567.0 μmol g^{-1} due to simultaneously enhanced hydrogenation of light olefins (Table S3). The BTX fraction in aromatics (BTX/Aro.) decreases from 61.1% to 43.4%, as the density of strong Brønsted acid sites increases from 60.8 to 231.8 μmol g^{-1}, and then levels off. ZSM-5-360 with a density of Brønsted acid sites of 60.8 μmol g^{-1} exhibits the highest BTX selectivity of 40.7% (Figure 5b).

2.5 Optimization of reaction conditions and the stability

Catalytic performance can be further improved by varying the reaction conditions. As shown in Figure 6a, a higher pressure facilitates CO conversion, but has little effect on the hydrocarbon distribution. For example, by increasing reaction pressure from 2 to 5 MPa, CO conversion is enhanced

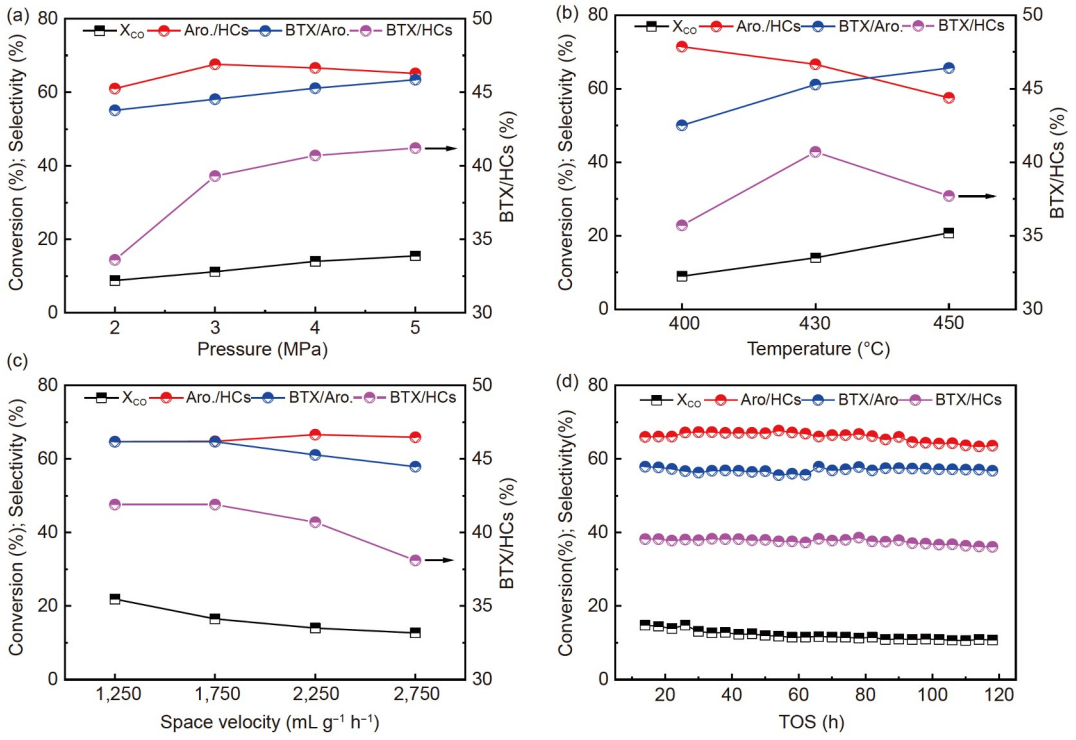

Figure 6 (a–c) Effects of reaction conditions on the catalytic performance: (a) pressure; (b) temperature and (c) space velocity. (d) Stability test of MnCr-SAPO-34-ZSM-5. Reaction conditions: 4.0 MPa, 430 °C, GHSV = 2,250 mL g^{-1} h^{-1}, H_2/CO/Ar = 47.5/47.5/5, MnCr/SAPO-34/ZSM-5 = 1/1.5/1.5 unless otherwise stated. See Tables S4–S6 for detailed hydrocarbon distributions. SAPO-34 and ZSM-5 were SAPO-34-0.1 (SiO_2/Al_2O_3 = 0.1) and ZSM-5-360 (SiO_2/Al_2O_3 = 360), respectively (color online).

from 8.8% to 15.5%. The selectivity of aromatics (Aro./HCs) and the BTX fraction among aromatics (BTX/Aro.) keep at around 68% and 60%, respectively. A higher reaction temperature is also beneficial for CO conversion but at the expense of aromatics selectivity (Figure 6b). When the space velocity is reduced to 1,250 from 2,750 mL g^{-1} h^{-1}, CO conversion increases to 21.9% (Figure 6c). The hydrocarbon distribution is not affected obviously while the BTX fraction increases from 57.8% to 64.7% and the corresponding BTX selectivity in hydrocarbons (BTX/HCs) increases from 38.1 to 41.9% (Figure 6c). CO conversion can be enhanced to 28.7% by increasing the ratio of oxide to zeolite to 1/1 at the space velocity of 1,250 mL g^{-1} h^{-1} (Figure S5 and Table S7), and further to 31.5% by decreasing the space velocity to 750 mL g^{-1} h^{-1} with the BTX fraction maintaining above 60% (Table S7). Figure 6d shows the stability of MnCr-SAPO-34-ZSM-5. CO conversion slight decreases from 14.8% to 10.8% during 120 h time on stream (TOS), while the selectivity of aromatics and the BTX fraction both remained rather stable. To get an insight on the loss of activity, we performed XRD, NH_3-TPD, N_2 physisorption and TG analysis. XRD patterns (Figure S6a and S6b) show that the MnCr oxide was turned to a mixture of MnO and Cr_2O_3 after the reaction for 10 h (10 h-spent), with the crystal sizes of 9.5 and 17.8 nm, respectively. Upon the reaction for 120 h (120 h-spent), the crystal sizes of MnO and Cr_2O_3 increase to 12.1 and 18.2 nm, respectively (Table S9). N_2 physisorption indicates that the micropore surface area and micropore volume dramatically decrease after the reaction for 120 h, while the external surface area and mesopore volume change little (Table S8). This could be caused by carbonaceous species in the micropores of zeolites, which is validated by NH_3-TPD (Figure S6c) and TG analysis (Figure S6d). Therefore, the slightly decrease of CO conversion during the reaction could be ascribed to the gradually increased crystal size of MnCr oxide and the carbonaceous species accumulation in the micropore of zeolites.

2.6 Reaction mechanism over MnCr-SAPO-34-ZSM-5

Based on the above discussion, we propose a scheme of syngas conversion over the MnCr-SAPO-34-ZSM-5 ternary composite catalyst (Scheme 1). Syngas is first activated on the MnCr oxide, being converted to intermediates such as ketene. Ketene is converted to light olefins ($C_2^=$–$C_4^=$) over SAPO-34 and to aromatics over ZSM-5 while olefins can be also further converted to aromatics partly over ZSM-5. The methylation of BTX with ketene to form C_{9+} aromatics (A_{9+}) is inhibited due to the reduced ketene concentration by SAPO-34. Consequently, the hydrocarbon distribution is modulated towards BTX without sacrificing the total selectivity of aromatics.

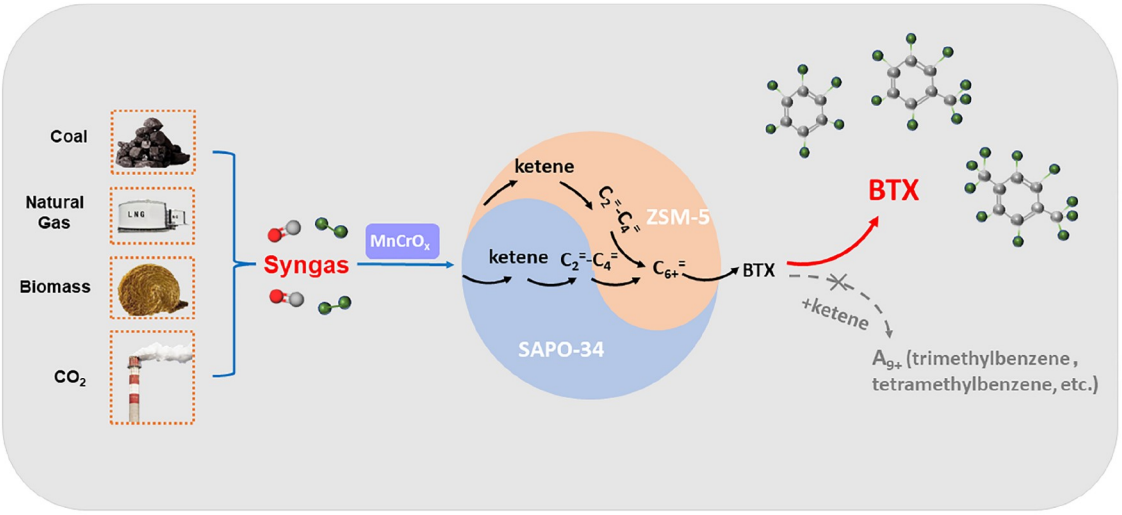

Scheme 1 Scheme for the syngas conversion to BTX with a proposed reaction pathway over MnCr-SAPO-34-ZSM-5 ternary composite catalyst (color online).

3 Conclusions

In summary, we design a ternary composite catalyst MnCr-SAPO-34-ZSM-5, which catalyzes the direct conversion of syngas into value-added BTX with a high selectivity. Under the reaction conditions of 430 °C, 4 MPa, and 1,250 mL g^{-1} h^{-1}, the BTX fraction reaches as high as 64.7% in aromatics, equivalent to a BTX selectivity 41.9% in hydrocarbons, at 21.9% CO conversion. A series of model reactions and characterization reveal that the presence of SAPO-34 plays an essential role by consuming partially ketene intermediate generated over MnCr oxides. Thus, further methylation of BTX by ketene is suppressed on the external surface of ZSM-5 zeolite, leading to an increased BTX fraction without sacrificing the overall aromatics selectivity. SAPO-34 in a close proximity with MnCr-ZSM-5 is much more beneficial for BTX formation. The simple catalyst design strategy provides an efficient method for the selective synthesis of BTX from syngas and it is expected to be applicable for CO_2 hydrogenation.

Acknowledgements This work was supported by the National Natural Science Foundation of China (22321002 and 22008234), the Natural Science Foundation of Liaoning Province (2022011086-JH3/107), Dalian High-level Talent Innovation Program (2021RQ111) and the Innovation Research Fund of Dalian Institute of Chemical Physics (DICP I202240).

Conflict of interest The authors declare no conflict of interest.

Supporting information The supporting information is available online at chem.scichina.com and link.springer.com/journal/11426. The supporting materials are published as submitted, without typesetting or editing. The responsibility for scientific accuracy and content remains entirely with the authors.

1 Qiao J, Wang J, Frenkel AI, Teng J, Chen X, Xiao J, Zhang T, Wang Z, Yuan Z, Yang W. *RSC Adv*, 2020, 10: 5961–5971
2 Shoinkhorova T, Cordero-Lanzac T, Ramirez A, Chung S, Dokania A, Ruiz-Martinez J, Gascon J. *ACS Catal*, 2021, 11: 3602–3613
3 Fu T, Guo Y, Li Z, Zhan G. *Fuel*, 2022, 315: 123241
4 Fu T, Shao J, Li Z. *Appl Catal B-Environ*, 2021, 291: 120098–120114
5 Zhao B, Zhai P, Wang P, Li J, Li T, Peng M, Zhao M, Hu G, Yang Y, Li YW, Zhang Q, Fan W, Ma D. *Chem*, 2017, 3: 323–333
6 Xu Y, Liu J, Ma G, Wang J, Lin J, Wang H, Zhang C, Ding M. *Fuel*, 2018, 228: 1–9
7 Xu Y, Liu J, Wang J, Ma G, Lin J, Yang Y, Li Y, Zhang C, Ding M. *ACS Catal*, 2019, 9: 5147–5156
8 Yang X, Wang R, Yang J, Qian W, Zhang Y, Li X, Huang Y, Zhang T, Chen D. *ACS Catal*, 2020, 10: 3797–3806
9 Xu Y, Ma G, Bai J, Du Y, Qin C, Ding M. *ACS Catal*, 2021, 11: 4476–4485
10 Yang J, Pan X, Jiao F, Li J, Bao X. *Chem Commun*, 2017, 53: 11146–11149
11 Fu Y, Ni Y, Chen Z, Zhu W, Liu Z. *J Energy Chem*, 2022, 66: 597–602
12 Cheng K, Zhou W, Kang J, He S, Shi S, Zhang Q, Pan Y, Wen W, Wang Y. *Chem*, 2017, 3: 334–347
13 Liu C, Su J, Liu S, Zhou H, Yuan X, Ye Y, Wang Y, Jiao W, Zhang L, Lu Y, Wang Y, He H, Xie Z. *ACS Catal*, 2020, 10: 15227–15237
14 Wang Y, Gao W, Wang K, Gao X, Zhang B, Zhao H, Ma Q, Zhang P, Yang G, Wu M, Tsubaki N. *Chem Sci*, 2021, 12: 7786–7792
15 Huang Z, Wang S, Qin F, Huang L, Yue Y, Hua W, Qiao M, He H, Shen W, Xu H. *ChemCatChem*, 2018, 10: 4519–4524
16 Zhou W, Shi S, Wang Y, Zhang L, Wang Y, Zhang G, Min X, Cheng K, Zhang Q, Kang J, Wang Y. *ChemCatChem*, 2019, 11: 1681–1688
17 Gilani SZA, Lu L, Arslan MT, Ali B, Wang Q, Wei F. *Catal Sci Technol*, 2020, 10: 3366–3375
18 Fu Y, Ni Y, Zhu W, Liu Z. *J Catal*, 2020, 383: 97–102
19 Miao D, Ding Y, Yu T, Li J, Pan X, Bao X. *ACS Catal*, 2020, 10: 7389–7397
20 Mitsuyoshi D, Kuroiwa K, Kataoka Y, Nakagawa T, Kosaka M, Nakamura K, Suganuma S, Araki Y, Katada N. *Microporous Mesoporous Mater*, 2017, 242: 118–126
21 Liang T, Toghiani H, Xiang Y. *Ind Eng Chem Res*, 2018, 57: 15301–15309
22 Jiao F, Pan X, Gong K, Chen Y, Li G, Bao X. *Angew Chem Int Ed*, 2018, 57: 4692–4696
23 Jiao F, Li J, Pan X, Xiao J, Li H, Ma H, Wei M, Pan Y, Zhou Z, Li M, Miao S, Li J, Zhu Y, Xiao D, He T, Yang J, Qi F, Fu Q, Bao X.

Science, 2016, 351: 1065–1068
24 Wang Y, Gao W, Kazumi S, Li H, Yang G, Tsubaki N. *Chem Eur J*, 2019, 25: 5149–5153
25 Zhu Y, Pan X, Jiao F, Li J, Yang J, Ding M, Han Y, Liu Z, Bao X. *ACS Catal*, 2017, 7: 2800–2804
26 Cheng K, Gu B, Liu X, Kang J, Zhang Q, Wang Y. *Angew Chem Int Ed*, 2016, 55: 4725–4728
27 Li J, Yu T, Miao D, Pan X, Bao X. *Catal Commun*, 2019, 129: 105711–105716
28 Li Z, Wang J, Qu Y, Liu H, Tang C, Miao S, Feng Z, An H, Li C. *ACS Catal*, 2017, 7: 8544–8548
29 Tuel A, Caldarelli S, Meden A, McCusker LB, Baerlocher C, Ristic A, Rajic N, Mali G, Kaucic V. *J Phys Chem B*, 2000, 104: 5697–5705
30 Marchese L, Frache A, Gianotti E, Martra G, Causà M, Coluccia S. *Microporous Mesoporous Mater*, 1999, 30: 145–153
31 Liu Y, Zhang L, Dong Z, Luo L. *Sci China Chem*, 2022, 65: 2015–2022
32 Martins GVA, Berlier G, Bisio C, Coluccia S, Pastore HO, Marchese L. *J Phys Chem C*, 2008, 112: 7193–7200
33 Zhai L, Zhang B, Liang H, Wu H, Yang X, Luo G, Zhao S, Qin Y. *Sci China Chem*, 2021, 64: 1088–1095
34 Li G, Jiao F, Pan X, Li N, Miao D, Li L, Bao X. *ACS Catal*, 2020, 10: 12370–12375
35 Wang CM, Wang YD, Xie ZK. *Catal Sci Technol*, 2016, 6: 6644–6649
36 Zhang Y, Gao P, Jiao F, Chen Y, Ding Y, Hou G, Pan X, Bao X. *J Am Chem Soc*, 2022, 144: 18251–18258
37 Rasmussen DB, Christensen JM, Temel B, Studt F, Moses PG, Rossmeisl J, Riisager A, Jensen AD. *Angew Chem Int Ed*, 2015, 54: 7261–7264
38 Chen W, Li G, Yi X, Day SJ, Tarach KA, Liu Z, Liu SB, Edman Tsang SC, Góra-Marek K, Zheng A. *J Am Chem Soc*, 2021, 143: 15440–15452